Scientific Research Publishing

Open Journal of Geology, 2026, 16(11), 765-790
https://www.scirp.org/journal/ojg
ISSN Online: 2161-7589
ISSN Print: 2161-7570

Factors Controlling Gold Mineralization at the Toéyoko Prospect (P17-P17 South), Bomboré District, Burkina Faso: A Structural and Host-Rock Lithogeochemical Approach

Madi Ouedraogo[1*], Gounwendmanaghré Hubert Zongo[1], Pascal Ouiya[2], Ernest Gomdebziige Ouedraogo[1], Saga Sawadogo[3], Seta Naba[3]

[1]Department of Mining Engineering, Université Yembila Abdoulaye TOGUYENI, Fada N'Gourma, Burkina Faso
[2]École Normale Supérieure, Institut de Formation et de Recherche en Sciences et Technologie, Ouagadougou, Burkina Faso
[3]Laboratoire Géosciences et Environnement, Université Joseph Ki-Zerbo, Ouagadougou, Burkina Faso
Email: *madisance1983@gmail.com

How to cite this paper: Ouedraogo, M., Zongo, G.H., Ouiya, P., Ouedraogo, E.G., Sawadogo, S. and Naba, S. (2026) Factors Controlling Gold Mineralization at the Toéyoko Prospect (P17-P17 South), Bomboré District, Burkina Faso: A Structural and Host-Rock Lithogeochemical Approach. *Open Journal of Geology*, **16**, 765-790.
https://doi.org/10.4236/ojg.2026.1611037

Received: October 15, 2026
Accepted: November 10, 2026
Published: November 13, 2026

Copyright © 2026 by author(s) and Scientific Research Publishing Inc.
This work is licensed under the Creative Commons Attribution International License (CC BY 4.0).
http://creativecommons.org/licenses/by/4.0/

Open Access

Abstract

Gold at the Toéyoko prospect (P17 and P17 South), south of the Bomboré deposit in Burkina Faso, is mainly hosted by silicified and deformed granitoids. To identify the factors controlling this mineralization, we combined 198 surface structural measurements, 2902 drill-core measurements from 43 diamond drill holes (848 measurements with a valid β angle) and geochemical analyses of 13 host-rock samples. At surface, the main foliation is subvertical and trends NNE-SSW (strike/dip 015/82); at depth, it dips 58˚ east (dip direction/dip 091/58) and is cut by NNW-SSE shear zones (075/61) that host quartz veins. At the scale of the permit, the foliation is fan-shaped. The angle between the mean foliation and shear-zone planes suggests mainly sinistral strike-slip movement (slip direction 355/17) during WNW-ESE shortening; because no paired S-C fabrics or kinematic indicators were measured, this sense of shear is provisional. The granitoids form two suites: a high-Sr/Y suite and a low-Al, Zr-rich (165 - 236 ppm) tonalitic to trondhjemitic suite; these names are provisional because alteration may have modified the major elements. Three of the four gold-bearing granitoids (5.1 - 8.6 g/t Au) belong to the Zr-rich suite, and all four are anomalous in As (>1000 ppm) and S (>0.4%). From this small, selected sample set, we propose a preliminary model in which transpression channeled fluids along the NNW-trending shear zones toward the contact between competent felsic intrusions and the surrounding metagabbros.

Keywords

Toéyoko Prospect, Orogenic Gold, Structural and Lithological Controls,

Oriented Drill Core, Zr-Rich Granitoids

1. Introduction

The Baoulé-Mossi domain of the Man-Leo Rise is one of the major Paleoproterozoic gold provinces [1] [2]. Its Birimian greenstone belts formed and were deformed during the Eburnean orogeny, between about 2.2 and 2.0 Ga [3]. Orogenic gold deposits are localized by shear zones and lithological contrasts [4]-[6]. In Burkina Faso, most large deposits lie along regional shear corridors such as the Markoye shear zone [4] [7].

The Bomboré deposit, mined by Orezone Gold Corporation about 85 km east of Ouagadougou, is a disseminated mineralization in strongly deformed greenstones, with albite, calcite, tourmaline, biotite and pyrite alteration. It is associated with a second-order structure of the Tiébélé-Dori-Markoye fault system [8]. Further south, at the Toéyoko prospect (P17 and P17 South showings), gold occurs mainly in silicified and deformed granitoids [8], but the factors that controlled its deposition have not been established. This paper sets out to identify them.

We first reconstructed the three-dimensional geometry of the structures from outcrop and oriented-core measurements and then worked out their kinematics. We used host-rock chemistry to characterize the mineralized unit. In the Discussion, we combine the two datasets into a genetic model to derive exploration criteria.

2. Geological Setting

2.1. The Baoulé-Mossi Domain

The Archean cores and the Paleoproterozoic Birimian terrains make up the West African Craton. The Baoulé-Mossi domain, beneath most of Burkina Faso, consists of volcano-sedimentary greenstone belts and large granitoid batholiths emplaced between about 2.2 and 2.07 billion years ago [3]. The early- to syntectonic tonalite-trondhjemite-granodiorite (TTG) series can be differentiated from the later potassic granites [7]. The belts extend in a NNE-SSW to NE-SW direction and are cut by regional shear zones that conveyed the mineralizing fluids [7] [9] [10]. Eburnean deformation began with shortening, folding, and thrusting, then progressed through a transcurrent stage to which most orogenic gold deposits are linked [4] [5] [9] (**Figure 1**). Recent studies describe the orogen as an anastomosing network of transpressional shear zones that accommodated distributed shortening and allowed the crust to move laterally and vertically. According to this interpretation, the majority of the large shear zones are transfer structures and not plate boundaries [6] [10]-[12].

2.2. Geology of the Bomboré District and the Toéyoko Prospect

The greenstone belt hosting the Bomboré deposit is 1 - 3 km wide and about 14 km long. Its strike swings from N040˚ in the north to N340˚ in the south around

late granitoid intrusions [8] [13]. It consists of greenschist-facies, locally amphibolite-facies, metavolcanic, and metasedimentary rocks, first intruded by tholeiitic gabbroic and ultramafic bodies and later by biotite granites, granodiorites, and quartz diorites [13]. The Toéyoko prospect lies on its southern extension. Metagabbros, metasedimentary rocks (arenites), and granodiorites crop out there, bounded to the west and south by large barren biotite-granite plutons [8]. The mineralized unit is a fine-grained, pre- to syntectonic microporphyritic granodiorite that also forms dykes and elongate intrusions elsewhere on the property [8]. We use "granodiorite" for this unit as it was mapped and logged; its major-element chemistry plots mainly in the fields of tonalites and trondhjemites, a classification that alteration may have modified (Sections 4.1 and 5.2). The Toéyoko exploration permit covers 63.41 km^2 (**Figure 1**).

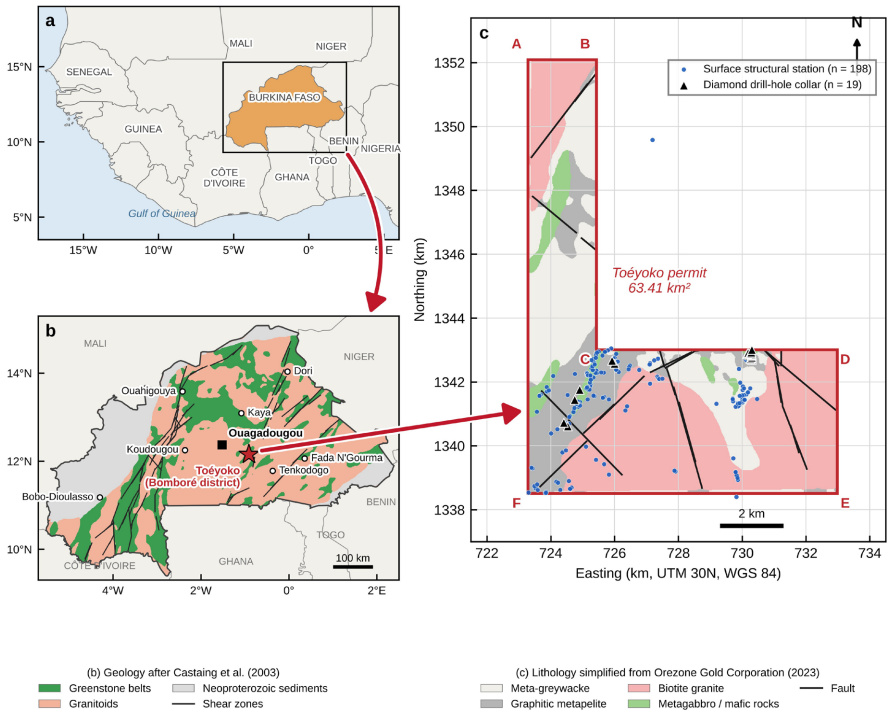


Figure 1. Location of the study area. (a) West Africa and position of Burkina Faso on the Man-Leo Rise; (b) Burkina Faso: simplified geology (after [14]), main towns and position of the Toéyoko prospect (Bomboré district); (c) Toéyoko permit (corners A-F; 63.41 km^2): simplified lithology and faults after Orezone Gold Corporation [8], surface structural stations and collars of the 19 oriented-core diamond drill holes. Red arrows link the position of Burkina Faso (a) to map (b), and the Toéyoko prospect (b) to the permit map (c). UTM coordinates, zone 30N, WGS 84; administrative boundaries from Natural Earth.

3. Materials and Methods

3.1. Structural Data Acquisition

We took surface measurements during lithostructural mapping on deformed rocks with a planar fabric. Of the 198 measurements, 195 are usable: 132 foliation strikes (127 with dip), 2 bedding measurements, and 61 quartz-vein strikes (6

with dip). We measured strike with a Brunton-type compass and dip with a clinometer, and located each station with a handheld GPS (**Figure 2(a)**, **Figure 2(b)**, **Figure 2(e)**, **Figure 2(f)**). At depth, we logged the oriented core of 19 diamond drill holes from the 2018 campaign (TYD0102 to TYD0120) following Orezone's structural logging procedure. For each plane, the α angle was read with a protractor ruler (**Figure 2(g)**) and the β angle with a core goniometer (**Figure 2(h)**), both from the reference line of the core (**Figure 2(c)** and **Figure 2(d)**). The α angle can be read on any core, whereas the β angle requires a core oriented with the Reflex system, which provides the reference line. We made 1195 measurements: 973 on foliation, 120 on quartz veins, 79 on shear zones and 23 on lithological contacts. The 13 holes in the eastern sector were drilled west, and the 6 holes in the western sector were drilled east. Their deviation, measured with a Reflex EZ-Trac magnetic tool and processed with the Reflex S-Process software, is

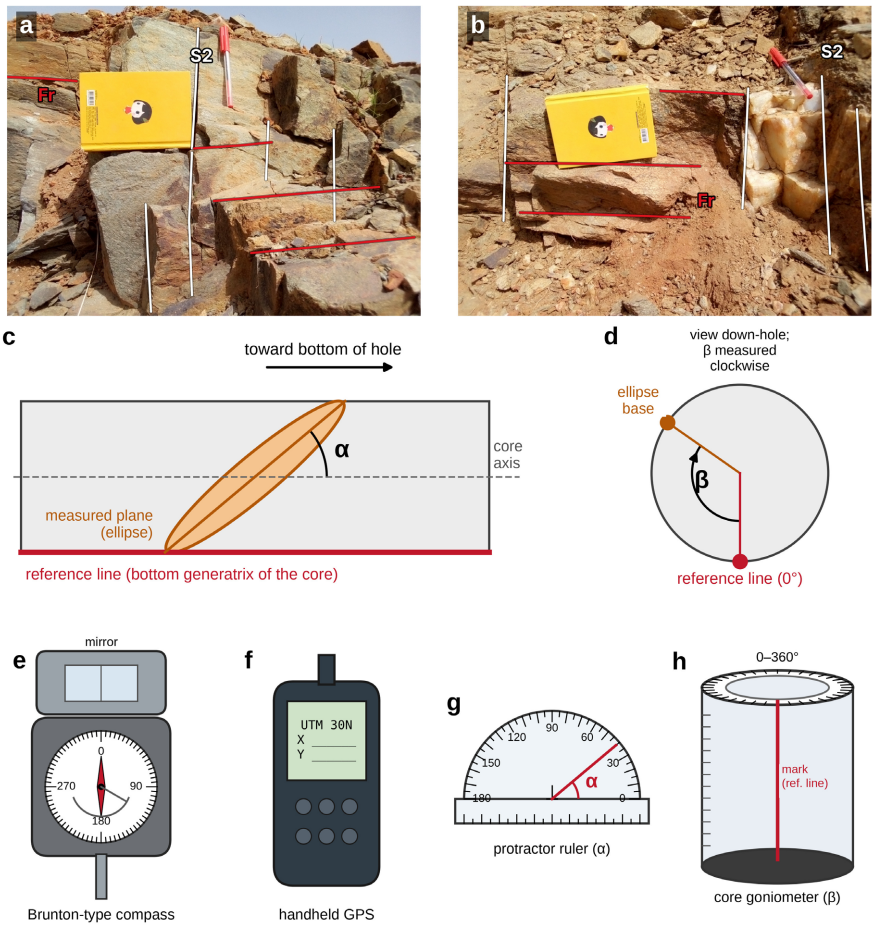


Figure 2. Structural data acquisition. (a, b) Subhorizontal outcrops of deformed granodiorite (field name; pen and notebook for scale): the main foliation S_2 (white lines; N-S to NNE strike, mean plane 015/82) is cut at right angles by E-W fractures (Fr, red lines); in (b), the quartz vein follows the S_2 plane; (c, d) α and β angles measured on oriented core following the Orezone procedure (side view and down-hole view; β is measured clockwise from the reference line); (e-h) measuring equipment (sketches): (e) Brunton-type compass with clinometer, (f) handheld GPS, (g) protractor ruler (α), (h) core goniometer (β).

less than 4˚ between collar and end of hole. Surface planes are given with the right-hand rule, and coordinates are in UTM (WGS 84, zone 30N). We added two further datasets: 958 measurements from 12 holes in the 2018 campaign north of this sector (BBD0989-BBD1000), 352 with a valid β angle, and 749 measurements from 12 holes in the 2013 campaign (TYD0004-TYD0015), 166 with a valid β angle. Table 1 gives the number of measurements in each dataset and shows how many of them are used in the orientation analysis.

Table 1. Drill-core structural datasets: number of measurements, measurements with a valid β, and measurements used to compute mean planes.

Dataset	Holes	Measurements	Valid β	Used for mean planes (Section 4.3)	Valid β not used
TYD0102-TYD0120 (2018), Toéyoko	19	1195	330	326: foliation 241, shear zones 45, contacts 9, veins 31	4 (western holes)
BBD0989-BBD1000 (2018)	12	958	352	351: foliation 271, shear zones 5, veins 75	1 (other structure type)
TYD0004-TYD0015 (2013)	12	749	166	141: foliation 71, shear zones 19, contacts 10, veins 41	25 (other structure types)
Total	**43**	**2902**	**848**	**818**	**30**

Measurements without a valid β ($\beta = 360^{\circ}$, the default entry value, or no β recorded) are 865, 606 and 583 in the three datasets. In the 2013 holes, orientations were calculated by Orezone from the planned hole orientations.

3.2. Conversion of Core Measurements and Statistical Treatment

The α angle is the acute angle between the core axis and the long axis of the ellipse that the plane traces on the core. The β angle is read clockwise, looking down-hole, from the reference line (bottom generatrix) of the core to the base of the ellipse (Figure 2(c) and Figure 2(d)). We converted the two angles to dip directions using vector calculations and interpolated the hole orientation between successive survey readings [15]. In the 2018 Toéyoko holes, 330 of the 1195 measurements have a valid β. We rejected 112 measurements with $\beta = 360^{\circ}$, the default entry value, and the other 753 have no usable β value. Of the 330 valid measurements, 326 come from the 13 eastern holes of the Toéyoko sector and define the mean planes given in Section 4.3; the remaining 4 come from the western holes and are too few to define a mean plane. In the western holes, the foliation is therefore assessed from α angles only (Section 4.3). Mean planes and girdle axes (β) come from the eigenvectors of the orientation tensor of the poles [16]. We contoured pole density using the Kamb method [17] and calculated mean strikes by doubling angles [18]. Rose diagrams are bidirectional and equal-area [19]. The uncertainty of a mean plane is reported as the half-apex angle of the 95% confidence cone (bootstrap, 1000 resamples). We processed the BBD holes the same

way. Where collar and downhole survey data were missing, we used the orientations that Orezone calculated from the planned hole orientations.

3.3. Lithogeochemistry

From core sections about 1 meter long, taken below the weathered zone at downhole depths of 45 to 169 m, thirteen fresh-rock samples were obtained: four metagabbros (GB1 to GB4), eight granitoids (GR1 to GR8), and one arenite (AR1). These samples were analyzed by SGS South Africa (Randfontein), a laboratory accredited to ISO/IEC 17025 by SANAS (number T0265; report RFT24-65463). The major elements were determined by X-ray fluorescence on beads fused with borate (method GO_XRF72; detection limit 0.01%), the loss on ignition was measured by calcination (method G_PHY01V), and the total carbon and sulfur contents were determined by combustion with infrared detection (method GE_CSA06V; detection limit 0.005%). For the trace elements, after digestion with four acids (HCl, HNO_3, HF, and $HClO_4$), the measurements were carried out by ICP-MS (GE_IMS40Q12) and ICP-OES (GE_ICP40Q12). The detection limits are 1 ppm for arsenic; 0.5 ppm for lead, copper and zirconium; 0.1 ppm for tungsten; 0.05 ppm for antimony, tellurium and molybdenum; 0.02 ppm for silver and hafnium; and 0.01 ppm for bismuth. When the arsenic concentration exceeds 10,000 ppm, it is not quantified. Since four-acid digestion does not completely dissolve refractory minerals such as zircon, the Zr and Hf values represent minimum concentrations. The gold grades for the same intervals, as determined by fire assay at SGS, are taken from the Orezone Gold Corporation drill-hole database and are available for all 13 samples. The rock types were assigned on the basis of the TAS diagram [20] [21] and the normative QAPF diagram [22] calculated from the CIPW norm [23]; the rare earth elements have been normalized to the CI chondrite as defined by Sun and McDonough [24]. The names of the rock types were checked at the drill-hole level using 1589 portable X-ray fluorescence analyses carried out by Orezone on fresh-rock core sections from the P17 South sector, with a Niton XL3t analyzer in soil mode (Standard Bulk Mode) after detector calibration, following Orezone's internal procedure. We have used only zirconium, titanium, iron and strontium, and only in relative terms, in accordance with the approach of SRK Consulting at Bomboré [25]. Portable XRF measures total Zr, whereas the laboratory values are partial (as explained above); the two datasets are therefore compared by means of element ratios and relative positions, not absolute concentrations.

Sampling and quality control. The 13 intervals were selected from six holes (see **Table 2**) to include the three logged lithologies (granitoid, metagabbro and arenite) and, for each of them, intervals both with and without significant gold grades in the Orezone database. This selection was intentional, and the samples do not form a statistically representative set for the prospect: the ratios of mineralized to barren samples in each group (Section 4.1) are not grade frequencies, and the results refer only to the sampled intervals. Suite A (Section 4.1) comes from a single hole (TYD0046), and four of the six Suite B samples come from holes BBD1000

and BBD1048, located north of the Toéyoko holes, so part of the difference between the two suites may be due to sampling location. No certified reference materials, blanks or duplicates of our own were added to the 13 samples. Quality control is based on the controls analyzed by the laboratory in the same batch and reported on certificate RFT24-65463: one blank, one replicate for each method, and the reference materials AMIS0807 (fusion XRF and LOI), AMIS0800 (C and S), OREAS 907, SU-1b and AMIS0355 (four-acid digestion). The blank is below or close to the detection limit for all elements (highest value 4 ppm Ba), which is negligible compared with the amounts found in the samples. The replicates agree within 1.5% for the major oxides (0.03 wt% for LOI), within 5% for C and S, and within 10% for most trace elements; As, Ag, Zr, Li and Be differ by 11% - 14%. Since the certificate does not provide the certified values of the reference materials, their recoveries are not reported here. For gold, the fire-assay grades are taken from the Orezone database; the quality-control results of the assay batches containing these 13 intervals were not available to us, and the QA/QC procedure applied by Orezone to its drilling is described in [8]. No check analyses were carried out at a second laboratory, and no interval was analyzed both by total (fusion) digestion and by four-acid digestion.

Table 2. Location of the analyzed samples (laboratory report RFT24-65463).

Sample	Rock type (this study)	Drill hole	Interval (m, down-hole)
GB1	Tholeiitic metagabbro	TYD0036	97 - 98
GB2	Differentiated/silicified metagabbro	TYD0036	89 - 90
GB3	Tholeiitic metagabbro	TYD0110	107 - 108
GB4	Differentiated/silicified metagabbro	TYD0110	89 - 90
GR1	Granitoid, Suite B	BBD1000	152 - 153
GR2	Granitoid, Suite A	TYD0046	63.6 - 64.7
GR3	Granitoid, Suite B	BBD1048	79 - 80
GR4	Granitoid, Suite B	BBD1000	168 - 169
GR5	Granitoid, Suite A	TYD0046	67 - 68
GR6	Granitoid, Suite B	TYD0023	45 - 46
GR7	Granitoid, Suite B	BBD1048	61 - 62
GR8	Granitoid, Suite B	TYD0023	46 - 47
AR1	Arenite (greywacke)	TYD0023	84 - 85

GR, granitoid; GB, metagabbro; AR, arenite. Holes BBD1000 and BBD1048 lie north of the Toéyoko holes; BBD1000 is part of the BBD0989-BBD1000 structural dataset (Section 3.1).

3.4. Structural Modeling and Kinematic Analysis

From the surface measurements on deformed rocks, we calculated foliation trajectories and dip domains over the entire permit area using Gaussian weighting (σ = 700 m) and an analysis radius of 1.2 km around each measurement point. A cross-

section was prepared from the apparent dips and the drill-hole data. The direction and sense of slip on the shear zones were estimated from the S-C geometry of the mean planes: the slip direction is the line in the C plane at right angles to the intersection of S and C, and the sense of slip follows from the rotation of S toward C [26] [27]. No paired S and C planes were measured on the same core intervals, and no kinematic indicators (shear bands, asymmetric porphyroclasts, slickenlines) or lineations were logged. Pooled mean planes are therefore used: the mean foliation plane of the Toéyoko sector (n = 241) as S and the mean shear-zone plane (n = 45) as C. The sense and direction of slip obtained in this way are inferred, not observed. We took the foliation pole to indicate the direction of greatest shortening.

4. Results

4.1. Nature and Composition of the Host Rocks

All samples are subalkaline (**Figure 3(a)**). Metagabbros GB1 and GB3 (SiO_2 = 48.0 - 49.5 wt%) have flat rare earth element (REE) patterns ($(La/Yb)_N$ = 1.8 - 2.5) of tholeiitic type. GB2 and GB4 contain more silica (60.4 - 63.3 wt%) and are differentiated or silicified equivalents. In the normative diagrams, the granitoids plot as tonalites and trondhjemites, apart from two granodiorites (GR4 and GR5), and sodic plagioclase makes up most of the feldspar (P/(A + P) = 86% - 99%) (**Figure 3(b)**). These names rest on major elements. Silicification adds SiO_2, and alkali alteration (albitization, sericitization) changes Na_2O and K_2O, so the TAS and normative classifications may not record the primary igneous composition. Sampling below the weathered zone removes the effect of supergene weathering but not that of hydrothermal alteration, which affects most of the mineralized samples. We therefore use the rock names as provisional labels and give more weight to elements that are relatively immobile during alteration (Ti, Zr, Y and the REE) [28].

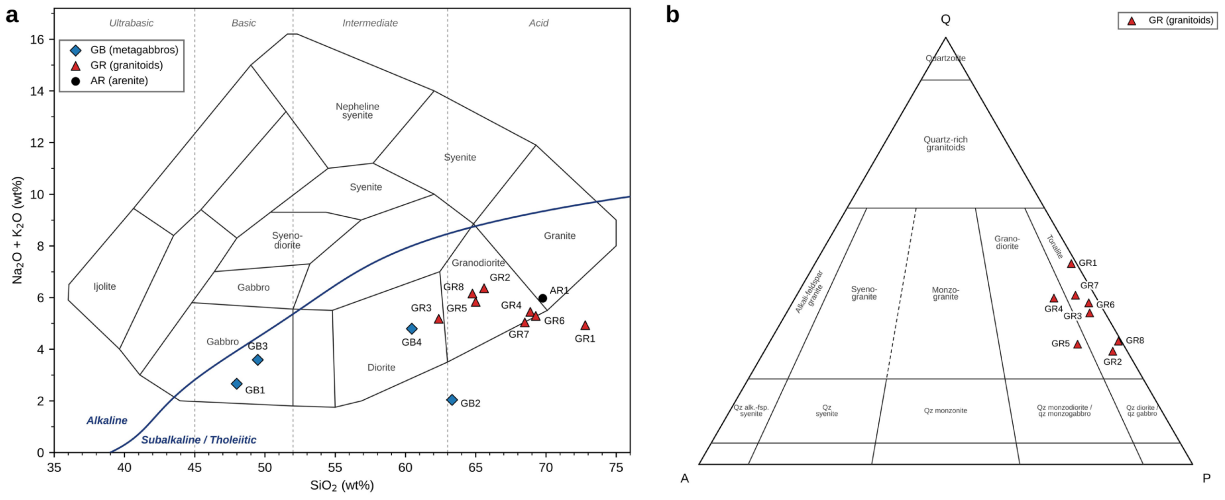


Figure 3. Classification diagrams used on the Toéyoko host rocks. (a) TAS diagram as given by Cox *et al.* [20], the plutonic version of Wilson [23], with the alkaline/subalkaline boundary defined by Irvine and Baragar [29], with the fields of the host rocks; (b) normative QAPF diagram of the granitoids [22], calculated from the CIPW norm, showing the tonalite and granodiorite fields.

The trace elements allow the two granitoid suites to be distinguished (see Figure 4 and Table 3). Suite A (GR2, GR5) is characterized by fractionated rare earth element patterns ($(La/Yb)_N$ = 8.7 - 8.8), low concentrations of the heavy rare earth elements (Y = 9 - 11 ppm), the absence of a europium anomaly, and high Sr/Y ratios (22 - 44), features that resemble those of TTG-type magmas in equilibrium with residual garnet [30]. Sr is mobile during alteration, however, and the Sr/Y ratio of these samples should be used with caution. Suite B (GR1, GR3, GR4, GR6, GR7, GR8) has a low content of Al_2O_3 (8.8 - 11.3 wt%). Its rare earth element patterns are flat ($(La/Yb)_N$ = 2.4 - 3.7); it has high values of Y (32 - 76 ppm) and Zr (165 - 236 ppm), shows a negative europium anomaly (Eu/Eu* = 0.61 - 0.74), and has low Sr/Y ratios (2.7 - 5.0). These features resemble those of the low-alumina trondhjemites described by Barker [31], which develop in the presence of plagioclase. The low Al_2O_3 contents may, however, partly reflect dilution by added silica, and the Eu anomaly may have been modified by plagioclase alteration; the flat REE patterns and the high Y contents are less affected by these processes. The Zr/TiO_2 ratios also distinguish the two suites (134 - 143 for Suite A, 295 - 549 for Suite B) from the tholeiitic metagabbros (30 - 44). The arenite AR1 is an immature greywacke, and its rare earth element pattern is similar to that of Suite A, suggesting that it may derive partly from this suite.

Six samples are anomalous in As (>1000 ppm) and S (>0.4%): four granitoids (GR1, GR2, GR3 and GR8) and two metagabbros (GB2 and GB4) (Figure 5).

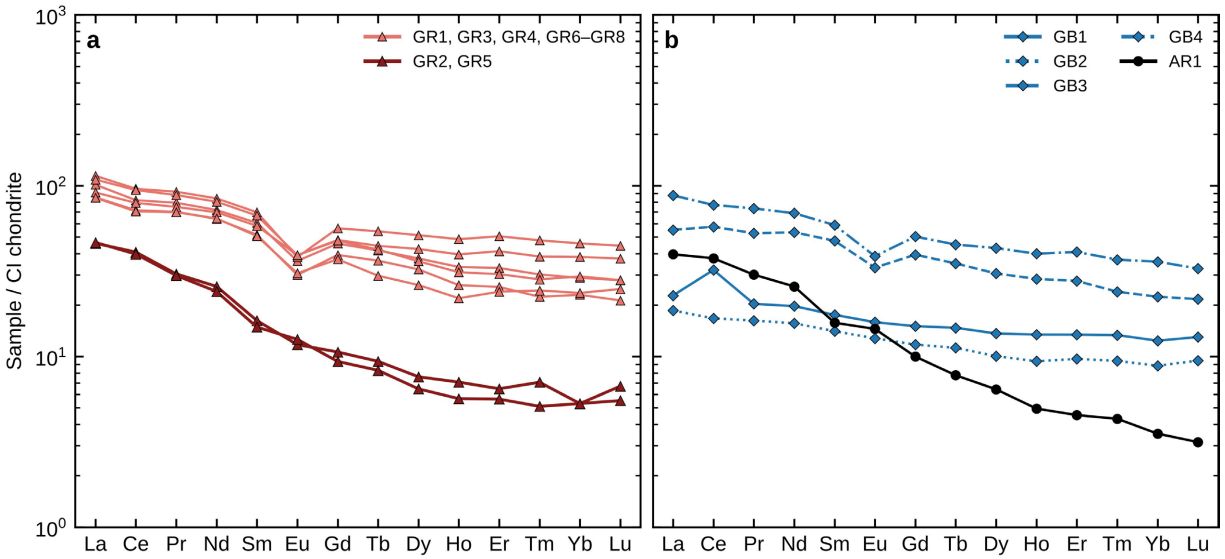


Figure 4. CI chondrite-normalized REE patterns [24]. (a) Granitoids of Suite A (GR2, GR5) and Suite B (GR1, GR3, GR4, GR6-GR8); (b) metagabbros and arenite AR1.

Table 3. Geochemical characteristics of the rock types of the Toéyoko prospect (ranges).

Rock type	Samples	SiO_2 (wt%)	Al_2O_3 (wt%)	Zr (ppm)	Y (ppm)	Sr/Y	$(La/Yb)_N$	Eu/Eu*	Zr/TiO_2	As (ppm)	Au (g/t)
Tholeiitic metagabbros	GB1, GB3	48.0 - 49.5	11.2 - 12.2	52 - 82	21 - 43	3.3 - 10.5	1.8 - 2.5	0.76 - 0.98	30 - 44	125 - 330	0.001

Continued

Differentiated/ silicified metagabbros	GB2, GB4	60.4 - 63.3	5.4 - 11.5	46 - 153	15 - 61	4.3 - 12.0	2.1 - 2.4	0.71 - 0.99	39 - 166	1220 - ≥10,000	0.84 - 8.12
Granitoids, Suite A (high Sr/Y)	GR2, GR5	65.0 - 65.6	12.7 - 13.9	67 - 76	9 - 11	22 - 44	8.7 - 8.8	0.89 - 1.07	134 - 143	72 - 2245	0.001 - 1.14
Granitoids, Suite B, mineralized (high Zr-Y)	GR1, GR3, GR8	62.4 - 72.8	8.8 - 11.0	187 - 236	38 - 51	3.2 - 4.3	3.5 - 3.7	0.67 - 0.69	409 - 549	2370 - ≥10,000	5.15 - 8.64
Granitoids, Suite B, barren (high Zr-Y)	GR4, GR6, GR7	68.5 - 69.3	10.8 - 11.3	165 - 219	32 - 76	2.7 - 5.0	2.4 - 3.6	0.61 - 0.74	295 - 445	54 - 291	0.001 - 0.015
Arenite (greywacke)	AR1	69.8	13.6	71	7	35	11.2	1.16	132	85	0.002

$Eu/Eu* = \frac{Eu_N}{(Sm_N \times Gd_N)^{0.5}}$. The upper quantification limit for As is 10,000 ppm. Au: fire assay (Orezone database).

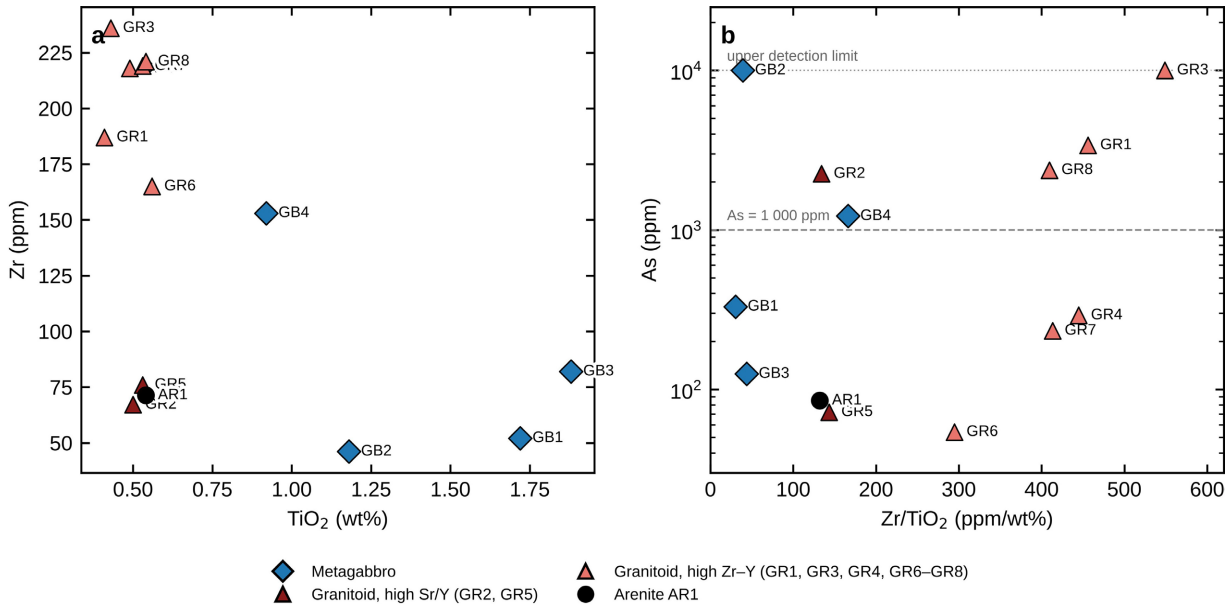


Figure 5. Geochemical parameters associated with gold mineralization in the host rocks (n = 13). (a) Zr versus TiO_2, separating the metagabbros, Suite A and the Zr-rich Suite B; (b) As versus Zr/TiO_2; three of the four granitoids anomalous in As (>1000 ppm) belong to Suite B.

Three of the four anomalous granitoids (GR1, GR3, GR8; As = 2370 to ≥10,000 ppm; S = 0.74% - 2.05%) belong to Suite B and have Zr/TiO_2 ratios above 400. The fourth, GR2 (As = 2245 ppm; S = 1.01%), belongs to Suite A. In contrast, GR4, GR6, and GR7 from Suite B are not anomalous (As = 54 - 291 ppm; S = 0.05 - 0.08%; Table 3), so rock composition alone cannot account for the mineralization. In each suite, half of the samples are gold-bearing (three of six in Suite B, one of two in Suite A), but the gold-bearing Suite B samples have higher grades (5.15 - 8.64 g/t) than the Suite A sample (GR2, 1.14 g/t). Gold grades are distributed in the same way as As and S. Samples anomalous in As and S assay 0.84 to 8.64 g/t Au (GR1: 8.64; GB4: 8.12; GR3: 5.82; GR8: 5.15; GR2: 1.14; GB2: 0.84), while the others, with less than 1000 ppm As and less than 0.25% S, do not exceed 0.015 g/t

(Figure 5(b)). Every gold-bearing sample contains at least 0.41% S, enough for the pyrite and arsenopyrite that host the gold, compared with no more than 0.23% in barren samples. With only 13 samples, this threshold is indicative. High As does not follow silica: As and SiO_2 are not correlated in the sample set (Spearman's $\rho = -0.24$). The mineralized metagabbros (GB2 and GB4) are the only samples clearly richer in silica than their barren equivalents (SiO_2 = 60 - 63 wt% vs 48 - 50 wt%), which we attribute to silicification.

The portable X-ray fluorescence data support these rock names throughout the area (see Figure 6). In the binary diagrams employed by SRK Consulting at Bomboré [25], the three lithologies recorded by Orezone (designated MI3 for the metagabbros, S3 for the metasedimentary rocks and I1C for the granitoid) lie in

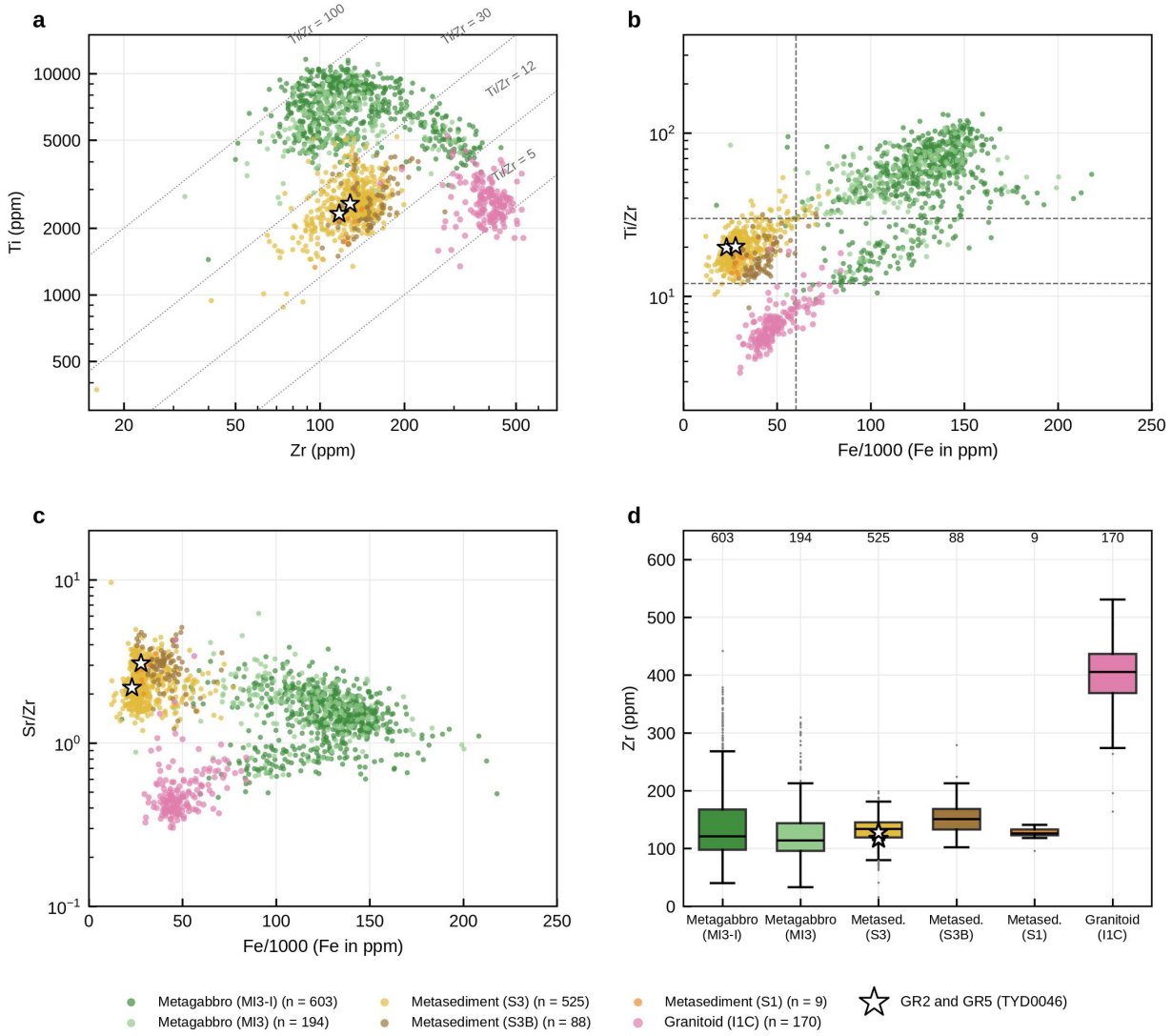


Figure 6. Binary plots of portable X-ray fluorescence analyses (Niton, Orezone) of 1589 fresh-rock core intervals from 21 drill holes in the P17 South sector, by logged lithology (I1C: granitoid; MI3: metagabbros; S3: metasedimentary rocks), following the approach of SRK Consulting [25]. (a) Ti versus Zr, with reference Ti/Zr ratios; (b) Ti/Zr versus Fe/1000; dashed lines: classification criteria (Ti/Zr = 12 and 30; Fe = 60,000 ppm); (c) Sr/Zr versus Fe/1000; (d) Zr content by lithology. Stars: intervals of samples GR2 and GR5 (drill hole TYD0046).

distinct fields. The metagabbros have a high content of Fe (median values ranging from 117 to 129 g/kg) and Ti (with a Ti/Zr ratio between 55 and 58). The metasedimentary rocks are low in Fe (28 - 40 g/kg), having a Ti/Zr ratio of 17 - 19 and a Sr/Zr ratio of 2.4 - 3.0. The I1C granitoid is characterized by a high Zr concentration (median 405 ppm; n = 170) and low Ti/Zr (6.4) and Sr/Zr (0.46). We tentatively correlate this population with the Zr-rich Suite B of the laboratory data. Its median Zr is about twice the Suite B range (165 - 236 ppm), which is expected if part of the zircon remained undissolved in the four-acid digestion (Section 3.3). The only intervals analyzed by both methods, those of GR2 and GR5, show the same offset: 117 - 128 ppm by portable XRF against 67 - 76 ppm in the laboratory, a ratio of 1.5 - 1.9, close to the ratio between the I1C median and the Suite B range (1.7 - 2.5). No Suite B interval has a matched portable XRF reading, so the correlation rests on relative Zr, Ti/Zr and Sr/Zr values and remains provisional. Simple cutoff criteria (for granitoids: Zr ≥ 250 ppm and Ti/Zr < 12; for metagabbros: Ti/Zr ≥ 30 and Fe ≥ 60,000 ppm; for metasedimentary rocks: Ti/Zr < 30 and Fe < 60,000 ppm) account for 89% of the 1589 fresh-rock intervals (96% for granitoids, 95% for metasedimentary rocks and 83% for metagabbros). At Bomboré, the agreement is only around 60% [25]. The GR2 and GR5 intervals fall into the metasedimentary field (Zr being 117 - 128 ppm; Ti/Zr approximately 20). Although we assign them to the granitoids on the basis of their CIPW norm and trace elements, further confirmation is required through thin section analysis.

4.2. Surface Structures

Foliation is the most common structure at surface. It is subvertical (median dip 75˚), with a mean strike of N016˚ (R = 0.76), a modal class of N020 - N030˚ and a mean plane of 015/82 (**Figures 7-9**). Its strike is similar in metagabbros (014/79), arenites (213/73) and granodiorites (005/86), although it dips west in the arenites; the granodiorites carry the same fabric, which indicates that the granodiorites were emplaced before or during deformation. In the arenites, bedding (210/75) parallels the foliation and has been transposed. The foliation strikes N025˚ in the western sector and N-S in the eastern sector, where it dips east everywhere. Across the permit, a dip-reversal zone separates a west-dipping domain in the southwest from the east-dipping domain that covers the rest of the area (**Figure 7**). Quartz veins have a mean strike of N031˚ (R = 0.68) and a second population striking N050˚-N070˚ (**Figure 8(c)**). E-W fractures also cut the foliation at right angles in outcrop (**Figure 2(a)**, **Figure 2(b)**), but they were not measured systematically.

4.3. Structures at Depth

In the Toéyoko sector the foliation, as measured on oriented core (n = 241), has a trend of N-S and a dip of 58˚ to the east (mean plane 091/58; principal eigenvalue 0.81). This same orientation is observed in the arenites (090/62; n = 101) and in the metagabbros (092/53; n = 133) (**Figure 10**). The shear zones (n = 45; mean plane 075/61) have a trend of NNW-SSE, being about 14˚ from the foliation, and

they cut through both the arenites and the metagabbros. Lithological contacts (080/68; n = 9) and the majority of the quartz veins (078/62; n = 31) are subparallel to the shear zones; only three of the veins dip gently (by 19˚ - 28˚). The poles to the foliation form a weak girdle with its axis (β) plunging 28˚ towards N161˚, this direction being parallel to the strike of the fabric and moderately inclined towards the SSE. The foliation becomes flatter with increasing depth, with median dips of 65˚ between 0 and 50 m down-hole, 64˚ between 50 and 100 m, 59˚ between 100

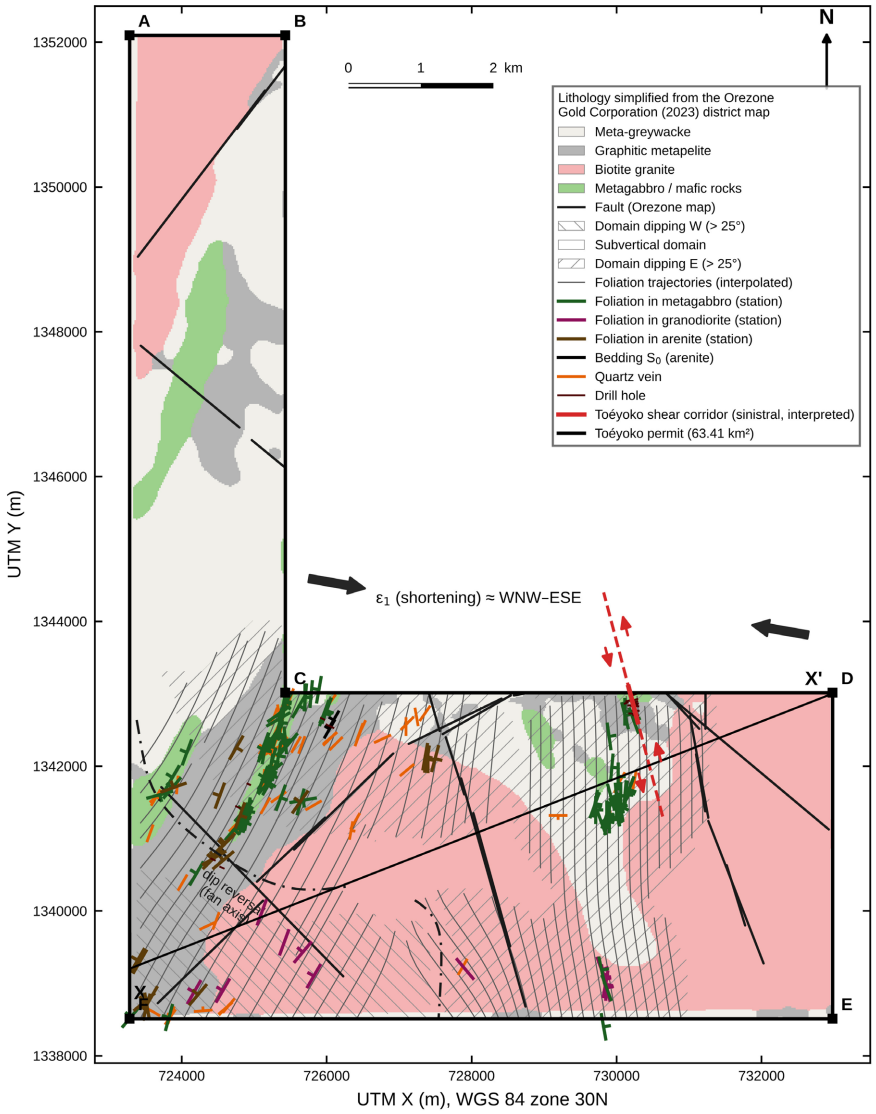


Figure 7. Interpretative lithostructural map of the Toéyoko permit (corners A-F; 63.41 km^2). Foliation trajectories and dip domains interpolated from measurements of structures visible at the surface in outcropping rocks; dash-dot line: dip reversal (fan axis); red line: Toéyoko shear corridor. This corridor does not crop out; we identified it from the shear zones intersected by all drill holes in the Toéyoko sector, measured on oriented core (Section 4.3), and then extended it along their mean strike; its sinistral sense, inferred from the S-C analysis of mean planes, is provisional. X-X′: trace of the interpretative cross-section presented in Section 4.4.

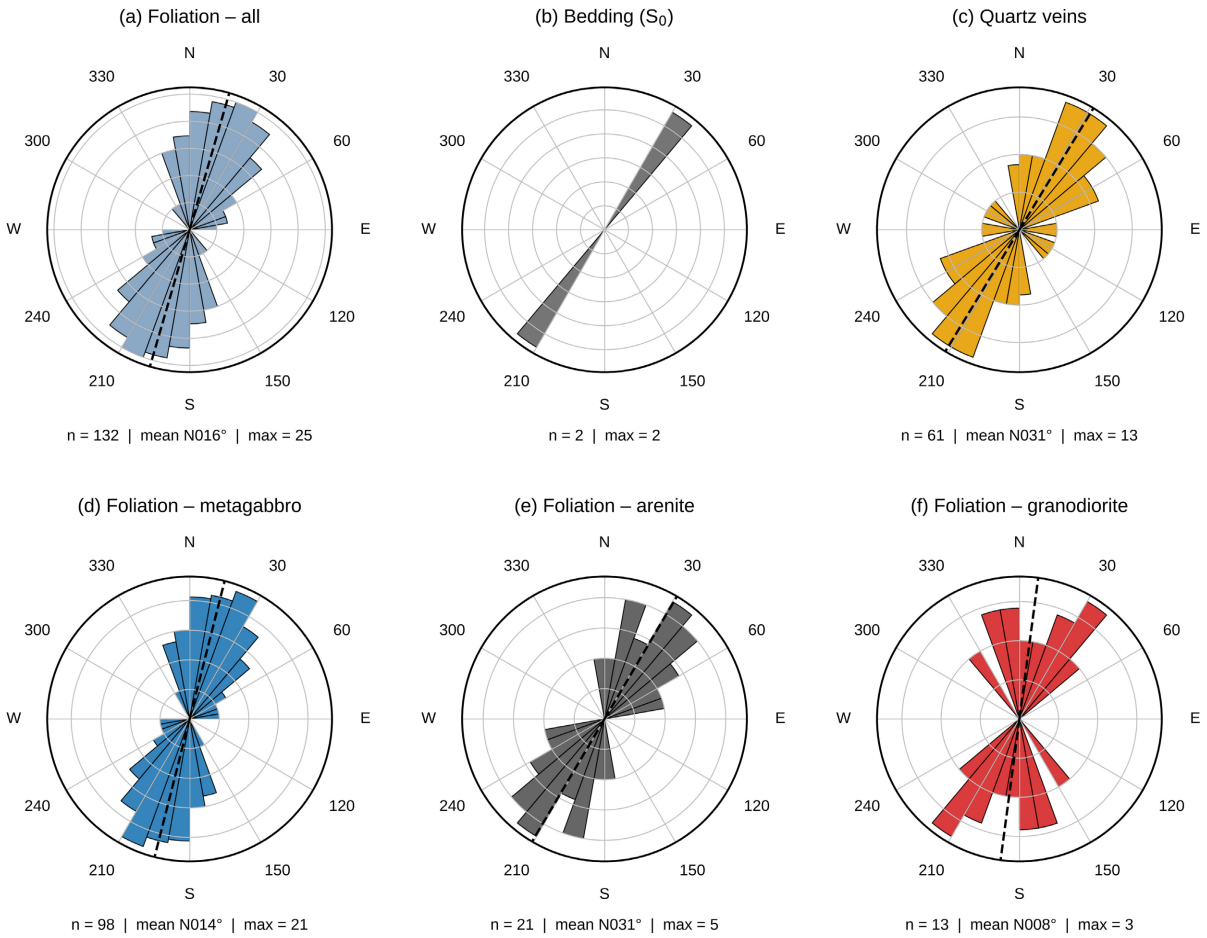


Figure 8. Bidirectional equal-area rose diagrams (10˚ classes) of surface structures: (a) foliation; (b) bedding; (c) quartz veins; (d-f) foliation in metagabbros, arenites and granodiorites.

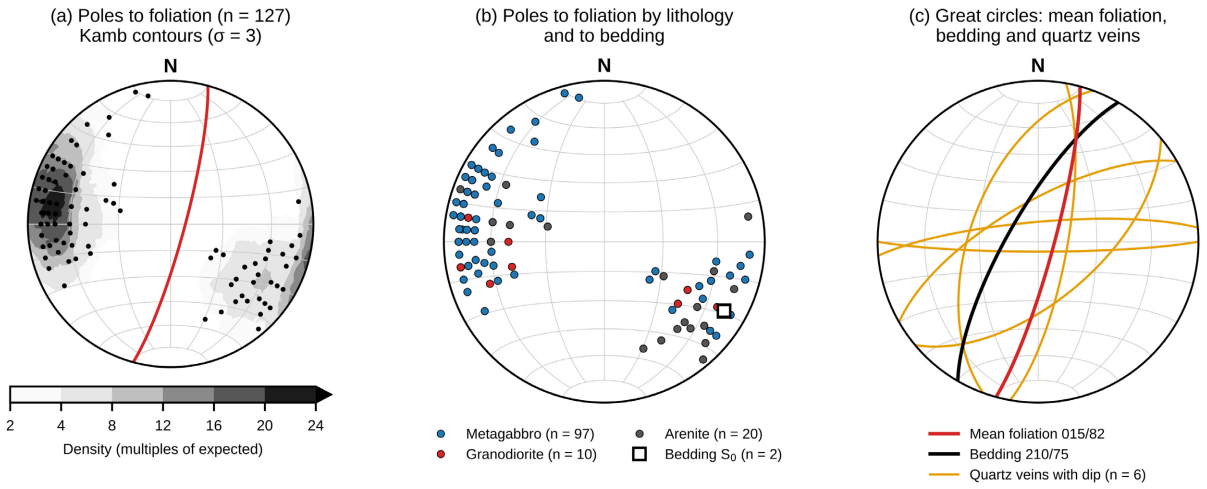


Figure 9. Stereograms of surface structures (Schmidt net, lower hemisphere): (a) poles to foliation and Kamb contours; (b) poles by lithology and poles to bedding; (c) mean planes of foliation and bedding, and veins with known dip.

and 150 m, and 52˚ below 150 m (n = 17). In the western holes the measured α angles (median 60˚) match only a foliation dipping 65˚ - 70˚ to the west, as at the

surface. Given the hole orientations from the downhole surveys, such a foliation would produce α angles of 59˚ - 61˚, against 10˚ - 18˚ for an east-dipping foliation (Table 4, line "West").

The other two drilling campaigns display the same geometry (Figure 11; Table 4). In the holes BBD0989 to BBD1000, which are up to 450 m north of the Toéyoko holes, the mean foliation plane is 086/65 (n = 271; 95% confidence cone: 3˚) and the mean vein plane is 089/60 (n = 75; 95% confidence cone: 7˚). The five oriented shear zones at 072/59 are 13˚ from the foliation plane and are close to the 14˚ value measured at Toéyoko. In the 2013 holes (TYD0004 to TYD0015) the foliation (083/53; n = 71; 6˚), the shear zones (082/49; n = 19; 11˚), the lithological contacts (078/51; n = 10) and the veins (090/48; n = 41; 10˚) strike N-S and dip 48˚ - 53˚ to the east, the shear zones being nearly parallel to the foliation (5˚). These 141 measurements are those plotted in Figure 11; the other 25 measurements with a valid β in the 2013 holes belong to other structure types that are not used in this analysis (Table 1). The mean foliation planes of the three datasets differ by 7˚ - 11˚ and dip 53˚ - 65˚ to the east. On the W-E cross-section of the Toéyoko sector (Figure 12), the foliation flattens with depth, as shown by the median dips given above.

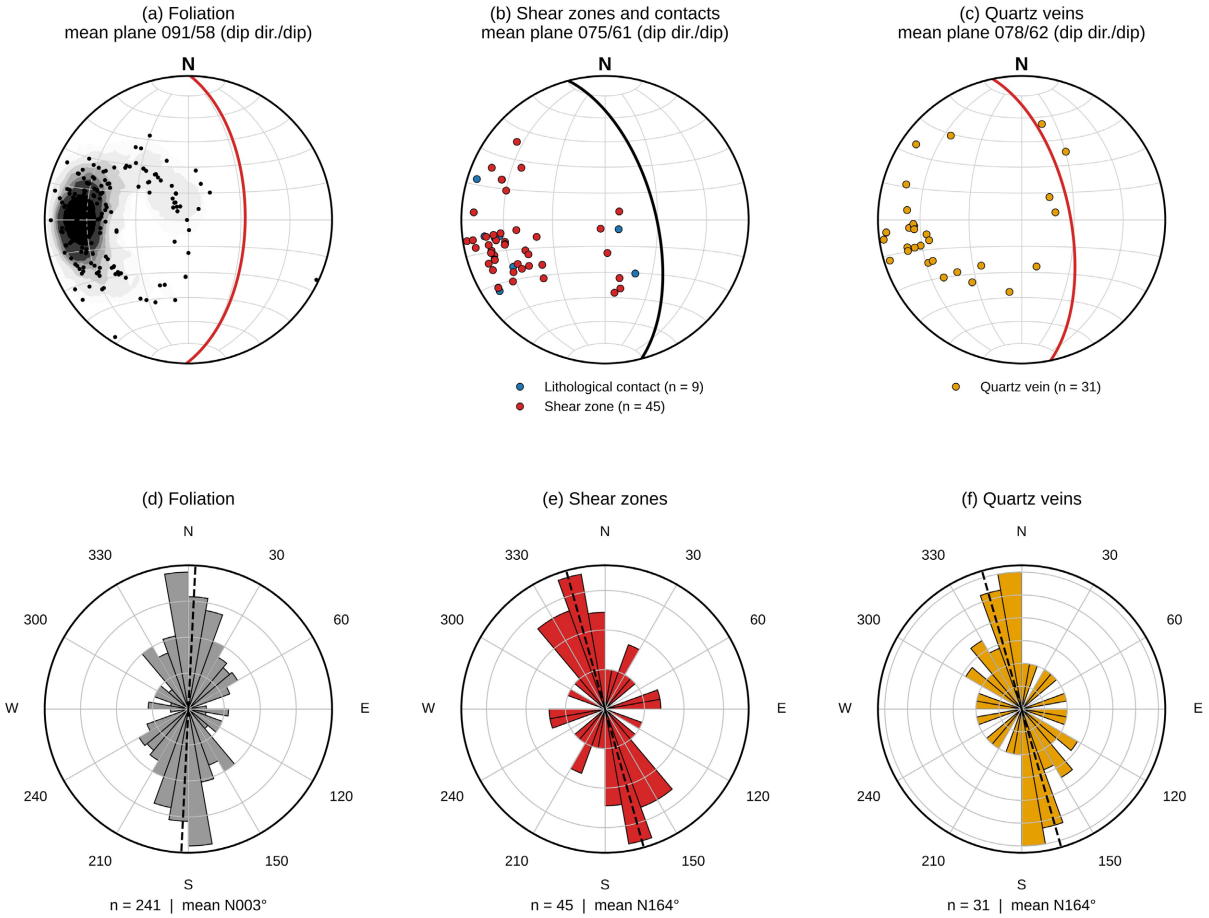


Figure 10. Orientation of structures measured on oriented core in the Toéyoko sector. (a-c) Poles to foliation (Kamb contours), shear zones and contacts, and quartz veins, with the mean plane (Schmidt net, lower hemisphere); (d-f) strike rose diagrams.

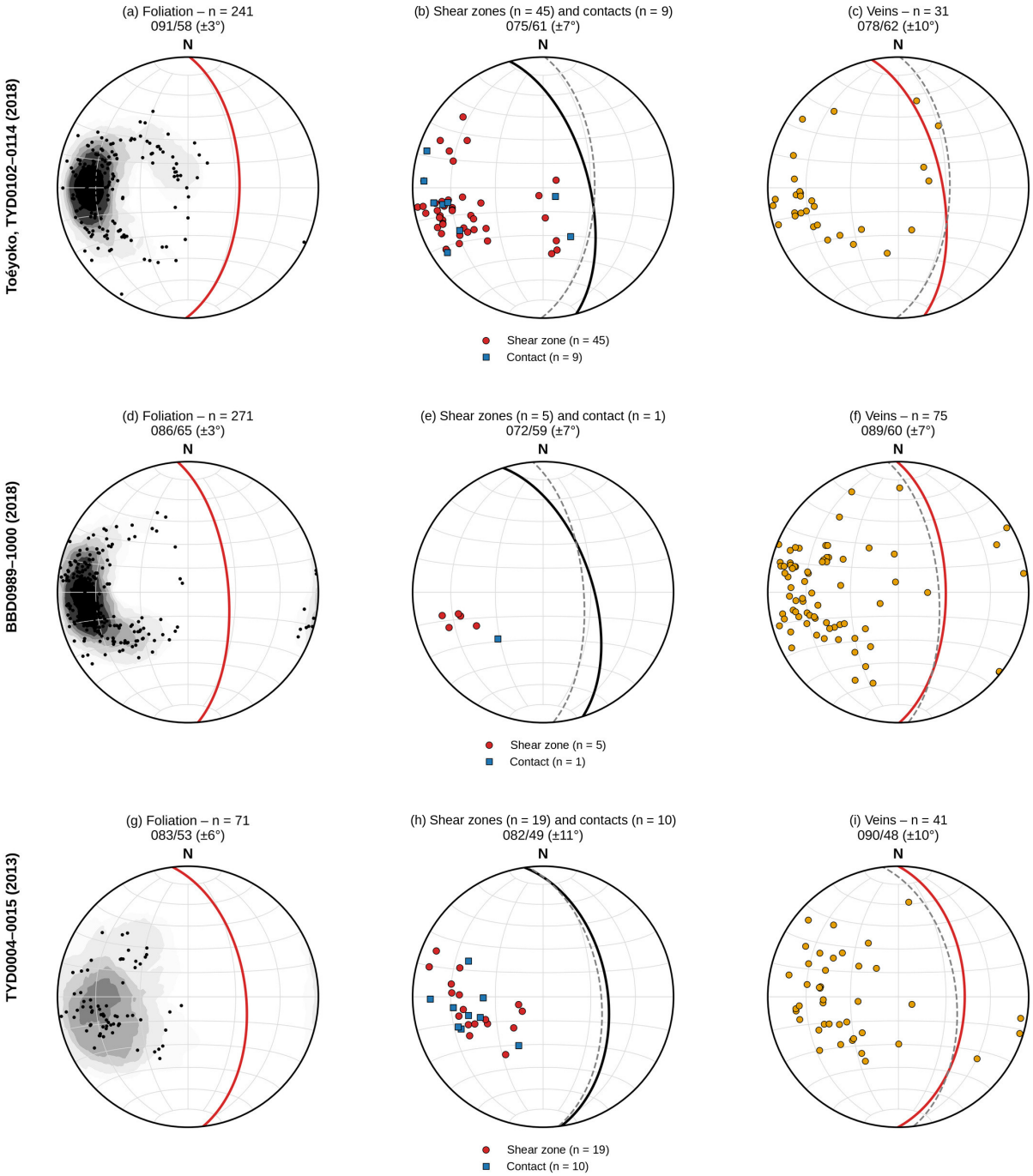


Figure 11. Comparison of structures measured on oriented core in the three datasets (Schmidt net, lower hemisphere): (a-c) Toéyoko sector, drill holes TYD0102-TYD0114 (2018); (d-f) drill holes BBD0989-BBD1000 (2018); (g-i) drill holes TYD0004-TYD0015 (2013; orientations calculated by Orezone from the planned hole orientations). Left: poles to foliation and Kamb contours; center: poles to shear zones and contacts; right: poles to veins. Solid line: mean plane (dip direction/dip), with the half-apex angle of the 95% confidence cone (bootstrap); dashed line: mean foliation plane.

Table 4. Orientation of structures at surface and at depth (strike by right-hand rule/dip; dip direction/dip in parentheses).

Structure	Sector	Surface	n	Depth	n	Source
Foliation	Toéyoko (east)	358/73	41	001/58 (091/58)	241	oriented core

Continued

Foliation	West (arenites)	213/73	20	≈180 - 235/65 - 70	239	α angles (model)
Foliation	BBD0989-BBD1000	—	—	356/65 (086/65)	271	oriented core
Foliation	TYD0004-TYD0015	—	—	353/53 (083/53)	71	oriented core*
Shear zones	Toéyoko (east)	—	—	345/61 (075/61)	45	oriented core
Shear zones	BBD0989-BBD1000	—	—	342/59 (072/59)	5	oriented core
Shear zones	TYD0004-TYD0015	—	—	352/49 (082/49)	19	oriented core*
Lithological contacts	Toéyoko (east)	—	—	350/68 (080/68)	9	oriented core
Quartz veins	Toéyoko (east)	N350 - N030	5	348/62 (078/62)	31	oriented core
Quartz veins	BBD0989-BBD1000	—	—	359/60 (089/60)	75	oriented core
Quartz veins	TYD0004-TYD0015	—	—	000/48 (090/48)	41	oriented core*
Bedding S_0	West (arenites)	210/75	2	—	—	—

Mean planes: principal eigenvector of the orientation tensor of the poles [16]. *Orientations calculated by Orezone from the planned hole orientations.

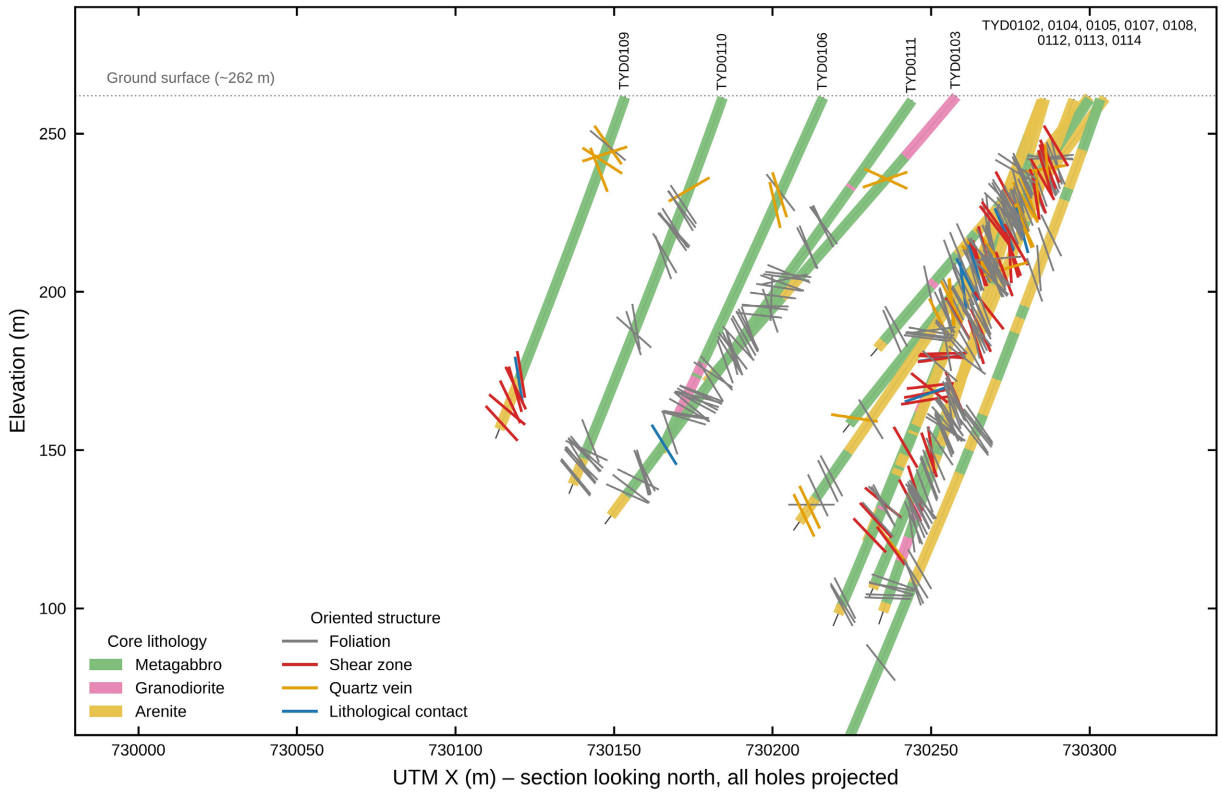


Figure 12. W-E cross-section (looking north) of the Toéyoko sector with projected drill holes; ticks show the apparent dip of oriented structures in the plane of the section.

4.4. Permit-Scale Geometry and Kinematics

On X-X′ (**Figure 13**) the foliation appears as a fan which opens upwards and dips west on the western side of the axis, east on the eastern side and is steepest

close to the axis. For the Toéyoko data, the S-C analysis of the mean planes (**Figure 14(a)**) places the S∩C intersection at 56˚ towards N112˚ and the slip direction at 355˚/17˚ in the shear plane. This geometry indicates mainly strike-slip movement with a small dip-slip component (17˚ plunge). Since the foliation is rotated clockwise with respect to the shear planes, the hanging wall would have moved north and the strike-slip component would be sinistral. Because S and C were not measured as pairs on the same core intervals (Section 3.4), this sense of shear and this slip direction are provisional; they need to be checked against kinematic indicators and lineations measured on oriented core. The pole to the foliation, 285/08 at the surface and 271/32 at depth, indicates near-horizontal WNW-ESE shortening.

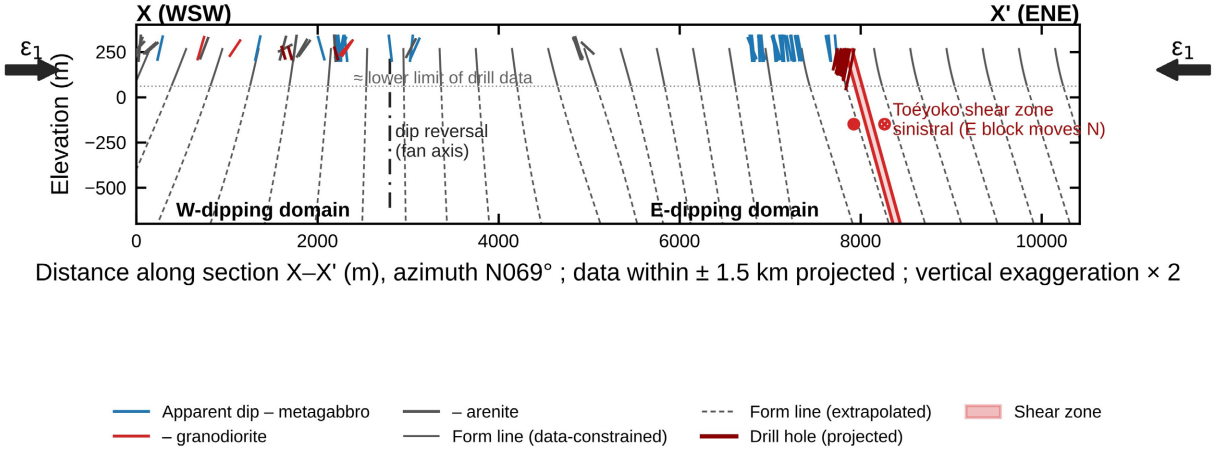


Figure 13. Interpretative cross-section X-X′ (azimuth N069˚) across the permit (vertical exaggeration ×2). Form lines constrained by data down to about 60 m elevation (solid lines) and extrapolated below (dashed lines); Toéyoko shear zone in red.

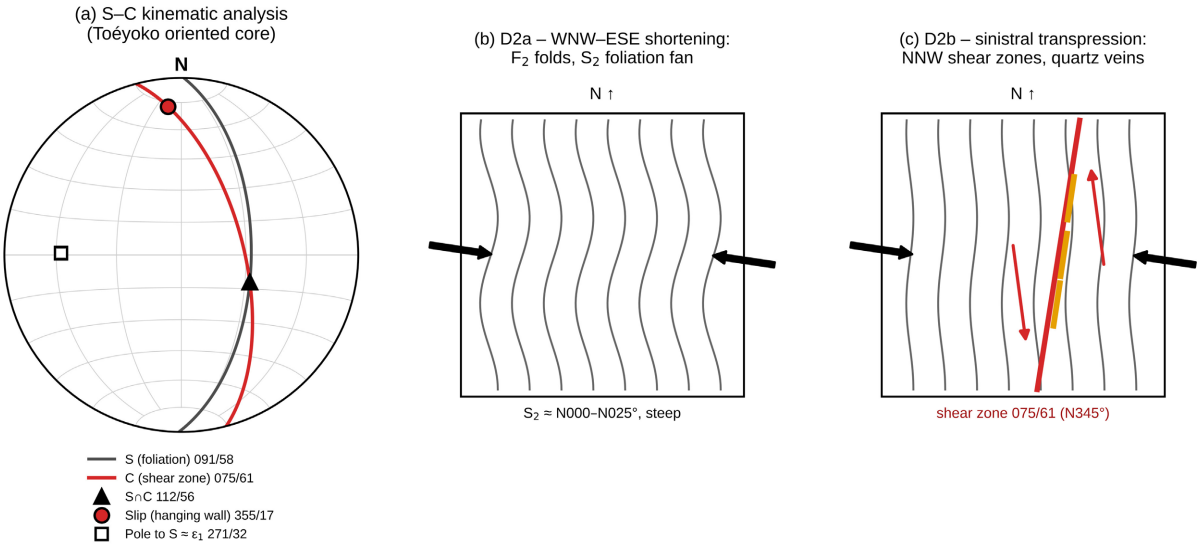


Figure 14. Kinematic analysis and evolution model. (a) Mean S and C planes measured on core (pooled mean planes, not paired observations), S∩C intersection, inferred slip direction of the hanging wall and pole to S; (b) stage D2a: WNW-ESE shortening and development of the S_2 foliation; (c) stage D2b: inferred sinistral transpression localized on vein-bearing NNW-SSE shear zones (provisional sense of shear).

5. Discussion

5.1. Deformation History

The deformation sequence we infer agrees with regional Eburnean models [7] [9]-[11] and with earlier work in the Bomboré mining area, which includes the Toéyoko prospect [8] [32] (**Table 5**). Bedding in the arenites is steep and parallel to the foliation and was transposed during the first phase (D1). We found no fabric or folds (F1) of this phase, probably because transposition erased them. The main planar fabric (S_2 foliation) strikes N-S to NNE-SSW, dips steeply, and formed during WNW-ESE shortening (D2; stage D2a, **Figure 14(b)**). At the P17 South showing, in the southern part of the Toéyoko prospect, Orezone mapped a foliation dipping about 55˚ ENE and parallel to the axial planes of isoclinal folds [8]. Lambert *et al.* [32] interpret it as an S_2 axial-planar cleavage of isoclinal F2 folds with N-S axial planes and hinges plunging 10˚ - 15˚ to the SSW. The β axis of our core data (28˚ toward N161˚) also indicates fold axes parallel to the foliation, but with a steeper plunge to the SSE, possibly because the hinges are curved. The girdle is weak (normalized eigenvalues of the orientation tensor of the poles: $\lambda_1 = 0.81$, $\lambda_2 = 0.11$ and $\lambda_3 = 0.08$), as expected for very tight folds with almost parallel limbs. At permit scale, the foliation fan could be a positive flower structure formed in transpression [33] or the core of a regional antiform. Similar anastomosing networks of foliation and shear zones have been described in Burkina Faso, where heterogeneous transpressional flow absorbs shortening and shear zones slightly oblique to the foliation transfer strain between domains [10] [11]. The Toéyoko shear zones, at about 14˚ to the foliation, appear to belong to this type.

Deformation later concentrated in east-dipping NNW-SSE shear zones (D2b; **Figure 14(c)**), which cut the foliation at a low angle. The S-C geometry of the mean planes suggests mainly sinistral movement on these shear zones. If this sense of shear is confirmed by kinematic indicators, WNW-ESE shortening continued with a strike-slip component, as sinistral transpression. Late brittle faults striking 070˚ and 110˚, seen on the magnetic surveys of the property [8], and an inferred E-W fault with apparent sinistral offset north of P17 [32] are assigned to D3. The E-W fractures seen in outcrop (**Figure 2(a)**, **Figure 2(b)**) and the N050-N070˚ veins measured at surface may belong to the same event.

Table 5. Summary of the deformation phases proposed for the Toéyoko prospect.

Phase	Regime	Structures	Evidence	Role in mineralization
D1	Early shortening	Tilting and transposition of bedding S_0; F1 folds not observed (probably obliterated by transposition)	S_0 (210/75)// foliation in arenites (213/73)	Set-up of the lithological architecture
D2a	WNW-ESE shortening	Isoclinal F_2 folds, N-S to NNE S_2 foliation, fan	Foliation 015/82 (surface), 091/58 (depth); β 161/28	Juxtaposition of competent felsic intrusions and metagabbros

Continued

D2b	Sinistral transpression (inferred)	NNW-SSE shear zones (075/61), quartz veins	S-C geometry of mean planes (provisional); slip 355/17, Section 4.4 and **Figure 14(a)**	Main episode of fluid flow and gold deposition
D3	Brittle faulting	Faults ≈ 070˚ and 110˚, sinistral E-W fault, E-W fractures, N050-N070˚ veins	Magnetic surveys; surface veins and fractures	Offset and local remobilization

D2a and D2b may represent two increments of a single progressive deformation.

5.2. Lithological Control

In our samples, the highest gold grades in granitoids occur in the low-Al, Zr- and Y-rich Suite B. This suite probably corresponds to the Zr-rich "granodiorite" that earlier studies [8] [32] identified as the host of the mineralization and whose Zr content was used to reinterpret several drill-hole logs [32]. The chemistry only partly supports the name given during core logging. In the normative QAPF diagram, the Suite B granitoids are tonalites, and only GR4 falls in the granodiorite field (**Figure 3(b)**). As noted in Section 4.1, these major-element names may have been shifted by silicification and alkali alteration, and sampling below the weathered zone does not ensure that the primary igneous chemistry is preserved. The tonalite-trondhjemite classification, and the comparisons of Suite A with garnet-bearing TTG sources and of Suite B with low-Al trondhjemites, are therefore working hypotheses that thin sections and less altered samples should test. We treat the unit as a tonalite-trondhjemite suite for descriptive purposes but keep the field name "granodiorite" on the maps and structural figures. Zr and the Zr/TiO_2 ratio, both relatively immobile [28], distinguish this unit from the metagabbros and from Suite A even where alteration has strongly changed the alkalis. Three of the six Suite B samples (GR1, 8.64 g/t; GR3, 5.82 g/t; GR8, 5.15 g/t) and one of the two Suite A samples (GR2, 1.14 g/t) are gold-bearing. The proportion of mineralized samples is thus the same in both suites, and the association with Suite B rests on grade, not on frequency. Two metagabbros (GB4, 8.12 g/t; GB2, 0.84 g/t) are also mineralized, while the Suite B granitoids without As and S anomalies (GR4, GR6, GR7) are barren (≤0.015 g/t). Because the 13 samples are few and were selected (Section 3.3), they cannot establish a lithological preference at the scale of the prospect; this would require a comparison of gold grades with the Zr-based lithology over the whole drill-hole database. The host lithology may favor mineralization but is not sufficient: gold occurs only where the fluids brought sulfur and produced sulfide alteration along the structural conduits.

The first difference between these intrusions and their host rocks is rheological. The quartz- and plagioclase-rich felsic granitoids are more competent than the chlorite-biotite metagabbros around them. During deformation, fracturing and dilation concentrate in the competent bodies, where fluids move more easily and

veins form [34] [35]. Their sodic character and iron content ($Fe_2O_3^T$ = 5.8 - 9.2 wt%) may also make them reactive toward sulfur-bearing fluids. Iron in the rock fixes sulfur as sulfides, breaking down gold-sulfur complexes and causing gold to precipitate [36].

5.3. Structural Control

We interpret the NNW-SSE shear zones as the main fluid pathways because they occur in all of the Toéyoko drill holes, host the majority of the quartz veins and intersect the lithological contacts at a shallow angle. Two further observations support a link between these structures and gold. All gold-bearing samples, whether granitoids or metagabbros, carry As and S anomalies (Section 4.1), which points to an external, sulfur-bearing fluid rather than to a control by host composition alone. The mineralized metagabbros are also the only silicified ones, which fits fluid flow focused along structures. The spatial relationship between gold intervals and logged shear zones has not yet been tested in the full drill-hole database; this test is the next step to support the model. In gold deposits associated with shear zones, ore shoots generally develop in dilational areas, the shape of which is determined by the direction of slip [34] [37]. If the movement at Toéyoko was mainly strike-slip, as the S-C analysis suggests, the dilational areas located at the bends in the shear planes would be elongated in a direction perpendicular to the slip and dip steeply near the S∩C intersection (112/56). Lambert *et al.* [32], on the other hand, link the grade envelopes to F2 folds that dip gently towards the SSW. The two geometries can coexist, with the F2 folds determining the shape of the host rock and their intersections with the shear zones determining where the high-grade shoots occur. Further drilling should check both plunge directions.

Two sections of the permit appear to be promising. One of these is the area in which the foliation changes from N025˚ in the west to N-S in the east, since this curvature could have led to the formation of dilational sites. The other is along the fan axis, since it is there that the fabric is steepest.

5.4. Uncertainties and Alternative Interpretations

The geochemical results rest on 13 samples selected to cover the main lithologies and both mineralized and barren intervals (Section 3.3), and Suite A is represented by a single hole. The two granitoid suites, the As and S thresholds and the association between Suite B and the highest grades are therefore preliminary. A larger sample set, taken at regular intervals along several holes and analyzed by total (fusion) digestion for Zr and the REE, together with portable XRF readings on the same intervals, would test the suites and thresholds and would calibrate the portable XRF data against the laboratory data.

The three-dimensional structural interpretation also has limits. The cross-section (**Figure 13**) is constrained by drill-hole data only down to about 60 m elevation, and the fan geometry below this level is extrapolated. The foliation trajecto-

ries (Figure 7) are interpolated from surface data with a Gaussian weighting of σ = 700 m, which smooths features smaller than a few hundred meters and leaves areas without outcrop unconstrained. In the western holes, the west-dipping foliation at depth is inferred from the fit between measured and modeled α angles, not measured directly. The 2013 orientations were calculated from the planned hole orientations, which may explain part of the 7˚ - 11˚ difference between the mean planes of the three datasets. The Toéyoko shear corridor does not crop out and is extended along strike from its drill-hole intersections. Finally, the kinematics come from pooled mean planes (Section 3.4).

Other interpretations remain possible. Because the foliation formed mainly during D2a, before the shear zones, its obliquity to the shear zones may reflect the initial geometry of the fabric rather than rotation during shearing; in that case the S-C angle would not record the sense of shear, and a dextral or mainly dip-slip movement could not be excluded. The foliation fan may be a positive flower structure [33] or the core of an antiform (Section 5.1), and data below 60 m elevation in the west are needed to separate the two. Gold could also postdate the main shear zones: gold associated with late- or post-orogenic deformation has been documented in the southern West African Craton [5] [38], and at Toéyoko the D3 fractures and N050-N070˚ veins have not been sampled. Finally, As- and S-rich silicified zones occur in both granitoids and metagabbros, so the fluid flux may have been the main control, with lithology acting mainly through its competence.

Our results can be compared with earlier work in the district. At Bomboré, gold is disseminated in strongly deformed greenstones with albite, calcite, tourmaline, biotite and pyrite alteration, along a second-order structure of the Tiébélé-Dori-Markoye system [8] [13]. Toéyoko differs in that most of the sampled gold is in felsic intrusions, but both share sulfide-rich alteration and a control by shear zones slightly oblique to the regional fabric. The N-S to NNE foliation and the steep fabric at depth agree with the S_2 axial-planar cleavage and isoclinal F2 folds described by Lambert *et al.* [32]; our results differ from theirs on the plunge of the ore shoots (Section 5.3). At the scale of Burkina Faso, the role of shear zones and lithological contrasts in localizing gold [4] [6] and the transpressional shear networks described by Chardon *et al.* [10] [11] are consistent with the model proposed here.

5.5. Exploration Model

At a regional level, we propose that the fluids flowed along a transpressional corridor associated with the Markoye system, probably with a sinistral component. In the prospect, shear zones that dip to the east and have a NNW-SSE trend localized the deformation and the formation of veins, and gold was deposited where these shear zones meet competent felsic intrusions, among which Suite B carries the highest grades in our samples. The targeting criteria derived from this preliminary model are given in Table 6; they should be tested by drilling and with the additional data listed in Section 5.4.

Table 6. Proposed targeting criteria for the Toéyoko prospect (preliminary).

Criterion	Measurable expression	Tool
Host unit	Granitoid with Zr > 160 ppm (four-acid ICP) or ≥ 250 ppm (portable XRF), Zr/TiO_2 > 290, Y > 30 ppm, $(La/Yb)_N$ < 4	Geochemistry (portable XRF, laboratory analyses)
Structural conduit	NNW-SSE shear zone dipping 60˚ - 65˚ to the east	Oriented core, mapping
Intersection site	Host unit/shear zone intersection; ore-shoot plunge to be tested (S∩C ≈ 112/56 or F_2 ≈ 10˚ - 15˚ SSW)	3D model, drilling
Regional setting	Foliation bend zone and fan axis	Interpretative structural map
Mineralization indicators	As > 1000 ppm, S > 0.4% (Au 0.8 - 8.6 g/t in the samples concerned; indicative thresholds, n = 13)	Geochemistry

6. Conclusion

Our data suggest that the Toéyoko gold mineralization formed where a favorable structural setting met a favorable host rock. The main fabric strikes N-S to NNE-SSW, dips steeply and formed during WNW-ESE shortening. It persists from the surface to at least 190 m down-hole (about 175 m vertical depth), is also found in drill holes up to 450 m further north and forms a fan at permit scale. NNW-SSE shear zones with a probable sinistral movement, inferred from mean planes, cut this fabric, carry the quartz veins and acted as fluid pathways. In our samples, the highest gold grades in granitoids occur in a low-Al, Zr- and Y-rich suite of tonalitic to trondhjemitic composition, which is more competent than the surrounding metagabbros and can be recognized by Zr/TiO_2 ratios above 290. With 13 selected samples, this association is not yet established at the scale of the prospect. The priority exploration target is the intersection between this unit, which can be traced geochemically, and the shear zones, whose orientation can be measured reliably only on oriented core. The model should first be tested with measurements of lineations and kinematic indicators on oriented core, then with a larger geochemical dataset (total digestion and matched portable XRF readings), a comparison of gold grades with Zr-based lithology and shear-zone intervals over the whole drill-hole database, and dating of the mineralization.

Author Contributions

Madi Ouedraogo: conceptualization, field mapping, core logging, data processing, formal analysis, writing (original draft). Gounwendmanaghré Hubert Zongo: supervision, interpretation of the geology of the Bomboré district, writing (review and editing). Pascal Ouiya: methodology, interpretation of the geochemical data, writing (review and editing). Ernest Gomdebziige Ouedraogo: validation, writing (review and editing). Saga Sawadogo: interpretation of the structural data, validation, writing (review and editing). Seta Naba: supervision, project administration,

writing (review and editing). All authors have read and approved the final version of the manuscript.

Conflicts of Interest

The authors declare no conflicts of interest regarding the publication of this paper.

References

[1] Milési, J.P., Ledru, P., Feybesse, J.L., Dommanget, A. and Marcoux, E. (1992) Early Proterozoic Ore Deposits and Tectonics of the Birimian Orogenic Belt, West Africa. *Precambrian Research*, **58**, 305-344. https://doi.org/10.1016/0301-9268(92)90123-6

[2] Goldfarb, R.J., André-Mayer, A., Jowitt, S.M. and Mudd, G.M. (2017) West Africa: The World's Premier Paleoproterozoic Gold Province. *Economic Geology*, **112**, 123-143. https://doi.org/10.2113/econgeo.112.1.123

[3] Parra-Avila, L.A., Kemp, A.I.S., Fiorentini, M.L., Belousova, E., Baratoux, L., Block, S., *et al.* (2017) The Geochronological Evolution of the Paleoproterozoic Baoulé-Mossi Domain of the Southern West African Craton. *Precambrian Research*, **300**, 1-27. https://doi.org/10.1016/j.precamres.2017.07.036

[4] Béziat, D., Dubois, M., Debat, P., Nikiéma, S., Salvi, S. and Tollon, F. (2008) Gold Metallogeny in the Birimian Craton of Burkina Faso (West Africa). *Journal of African Earth Sciences*, **50**, 215-233. https://doi.org/10.1016/j.jafrearsci.2007.09.017

[5] Masurel, Q., Eglinger, A., Thébaud, N., Allibone, A., André-Mayer, A., McFarlane, H., *et al.* (2022) Paleoproterozoic Gold Events in the Southern West African Craton: Review and Synopsis. *Mineralium Deposita*, **57**, 513-537. https://doi.org/10.1007/s00126-021-01052-5

[6] Perret, J., Jessell, M.W., Masurel, Q., Hayman, P.C., Thébaud, N., Baratoux, L., *et al.* (2025) Review of Paleoproterozoic Tectonics in the Southern West African Craton: Insights from Multi-Disciplinary Data Integration. *Precambrian Research*, **422**, Article ID: 107707. https://doi.org/10.1016/j.precamres.2025.107707

[7] Baratoux, L., Metelka, V., Naba, S., Jessell, M.W., Grégoire, M. and Ganne, J. (2011) Juvenile Paleoproterozoic Crust Evolution during the Eburnean Orogeny (~2.2-2.0Ga), Western Burkina Faso. *Precambrian Research*, **191**, 18-45. https://doi.org/10.1016/j.precamres.2011.08.010

[8] Orezone Gold Corporation (2023) Bomboré Phase II Expansion, Burkina Faso, West Africa: Definitive Feasibility Study. NI 43-101 Technical Report, Effective Date 28 March 2023. https://orezone.com

[9] Feybesse, J.L., Billa, M., Guerrot, C., Duguey, E., Lescuyer, J.L., Milési, J.P., *et al.* (2006) The Paleoproterozoic Ghanaian Province: Geodynamic Model and Ore Controls, Including Regional Stress Modeling. *Precambrian Research*, **149**, 149-196. https://doi.org/10.1016/j.precamres.2006.06.003

[10] Chardon, D., Bamba, O. and Traoré, K. (2020) Eburnean Deformation Pattern of Burkina Faso and the Tectonic Significance of Shear Zones in the West African Craton. *BSGF—Earth Sciences Bulletin*, **191**, Article 2. https://doi.org/10.1051/bsgf/2020001

[11] Chardon, D., Traoré, K., Gumiaux, C. and Naba, S. (2026) Transpressional Flow and Escape of Orogens: The Paleoproterozoic Eburnean Accretionary Orogen of West Africa. *Journal of Structural Geology*, **210**, Article ID: 105742. https://doi.org/10.1016/j.jsg.2026.105742

[12] Traoré, K., Chardon, D., Naba, S., Wane, O. and Bouaré, M.L. (2022) Paleoprotero-

zoic Collision Tectonics in West Africa: Insights into the Geodynamics of Continental Growth. *Precambrian Research*, **376**, Article ID: 106692. https://doi.org/10.1016/j.precamres.2022.106692

[13] Zongo, G.H. (2017) Caractérisation du gisement aurifère de Bomboré: pétrographie, géochimie, déformation, altération hydrothermale et minéralisation (Burkina Faso, Afrique de l'Ouest). Ph.D. Thesis, Université Ouaga I Pr Joseph Ki-Zerbo, Ouagadougou. (In French)

[14] Castaing, C., Billa, M., Milési, J.P., Thiéblemont, D., Le Métour, J., Egal, E., Donzeau, M., *et al.* (2003) Notice explicative de la carte géologique et minière du Burkina Faso à l'échelle 1/1,000,000. BRGM, 148 p. (In French)

[15] Marjoribanks, R. (2010) Geological Methods in Mineral Exploration and Mining. 2nd Edition, Springer. https://doi.org/10.1007/978-3-540-74375-0

[16] Woodcock, N.H. (1977) Specification of Fabric Shapes Using an Eigenvalue Method. *Geological Society of America Bulletin*, **88**, 1231-1236. https://doi.org/10.1130/0016-7606(1977)88<1231:sofsua>2.0.co;2

[17] Kamb, W.B. (1959) Ice Petrofabric Observations from Blue Glacier, Washington, in Relation to Theory and Experiment. *Journal of Geophysical Research*, **64**, 1891-1909. https://doi.org/10.1029/jz064i011p01891

[18] Mardia, K.V. and Jupp, P.E. (1999) Directional Statistics. Wiley. https://doi.org/10.1002/9780470316979

[19] Nemec, W. (1988) The Shape of the Rose. *Sedimentary Geology*, **59**, 149-152. https://doi.org/10.1016/0037-0738(88)90105-4

[20] Cox, K.G., Bell, J.D. and Pankhurst, R.J. (1979) The Interpretation of Igneous Rocks. George Allen & Unwin. https://doi.org/10.1007/978-94-017-3373-1

[21] Wilson, M. (1989) Igneous Petrogenesis: A Global Tectonic Approach. Unwin Hyman. https://doi.org/10.1007/978-1-4020-6788-4

[22] Le Maitre, R.W., Streckeisen, A., Zanettin, B., Le Bas, M.J., Bonin, B., Bateman, P., *et al.* (2002) Igneous Rocks: A Classification and Glossary of Terms. 2nd Edition, Cambridge University Press. https://doi.org/10.1017/CBO9780511535581

[23] Verma, S.P., Torres-Alvarado, I.S. and Velasco-Tapia, F. (2003) A Revised CIPW Norm. *Schweizerische Mineralogische und Petrographische Mitteilungen*, **83**, 197-216.

[24] Sun, S.S. and McDonough, W.F. (1989) Chemical and Isotopic Systematics of Oceanic Basalts: Implications for Mantle Composition and Processes. *Geological Society, London, Special Publications*, **42**, 313-345. https://doi.org/10.1144/gsl.sp.1989.042.01.19

[25] SRK Consulting (2010) Geochemistry Analysis, Bombore Project. Memo 3CO006.001 to Orezone Inc. SARL, 27 August 2010. SRK Consulting (Canada) Inc.

[26] Berthé, D., Choukroune, P. and Jegouzo, P. (1979) Orthogneiss, Mylonite and Non Coaxial Deformation of Granites: The Example of the South Armorican Shear Zone. *Journal of Structural Geology*, **1**, 31-42. https://doi.org/10.1016/0191-8141(79)90019-1

[27] Passchier, C.W. and Trouw, R.A.J. (2005) Microtectonics. 2nd Edition, Springer. https://doi.org/10.1007/3-540-29359-0

[28] MacLean, W.H. and Kranidiotis, P. (1987) Immobile Elements as Monitors of Mass Transfer in Hydrothermal Alteration; Phelps Dodge Massive Sulfide Deposit, Matagami, Quebec. *Economic Geology*, **82**, 951-962. https://doi.org/10.2113/gsecongeo.82.4.951

[29] Irvine, T.N. and Baragar, W.R.A. (1971) A Guide to the Chemical Classification of the Common Volcanic Rocks. *Canadian Journal of Earth Sciences*, **8**, 523-548. https://doi.org/10.1139/e71-055

[30] Moyen, J.-F. and Martin, H. (2012) Forty Years of TTG Research. *Lithos*, **148**, 312-336. https://doi.org/10.1016/j.lithos.2012.06.010

[31] Barker, F. (1979) Trondhjemite: Definition, Environment and Hypotheses of Origin. *Developments in Petrology*, **6**, 1-12. https://doi.org/10.1016/b978-0-444-41765-7.50006-x

[32] Lambert, C., Hales, M. and Koegelenberg, C. (2026) Structural Analysis and 3D Modelling, Bomboré Property, Orezone, Burkina Faso. TECT Geological Consulting, Report TECT003/2026P.

[33] Sanderson, D.J. and Marchini, W.R.D. (1984) Transpression. *Journal of Structural Geology*, **6**, 449-458. https://doi.org/10.1016/0191-8141(84)90058-0

[34] Robert, F. and Poulsen, K.H. (2001) Vein Formation and Deformation in Greenstone Gold Deposits. In: Richards, J.P. and Tosdal, R.M., Eds., *Structural Controls on Ore Genesis*, Society of Economic Geologists, 111-155. https://doi.org/10.5382/rev.14.05

[35] Cox, S.F. (2005) Coupling between Deformation, Fluid Pressures, and Fluid Flow in Ore-Producing Hydrothermal Systems at Depth in the Crust. In: Hedenquist, J.W., Thompson, J.F.H., Goldfarb, R.J. and Richards, J.P., Eds., *One Hundredth Anniversary Volume*, Society of Economic Geologists, 39-75. https://doi.org/10.5382/av100.04

[36] Mikucki, E.J. (1998) Hydrothermal Transport and Depositional Processes in Archean Lode-Gold Systems: A Review. *Ore Geology Reviews*, **13**, 307-321. https://doi.org/10.1016/s0169-1368(97)00025-5

[37] Sibson, R.H., Robert, F. and Poulsen, K.H. (1988) High-Angle Reverse Faults, Fluid-Pressure Cycling, and Mesothermal Gold-Quartz Deposits. *Geology*, **16**, 551-555. https://doi.org/10.1130/0091-7613(1988)016<0551:harffp>2.3.co;2

[38] Perret, J., Thébaud, N., Ribeiro, B.V., Tucker, N.M., Centrella, S., Koné, T.G., *et al.* (2026) P-T-t-D Constraints on Post-Orogenic Deformation and Coeval Mineralisation in the Archean-Paleoproterozoic Transition Zone of the Southern West African Craton. *Journal of Structural Geology*, **207**, Article ID: 105670. https://doi.org/10.1016/j.jsg.2026.105670